Enhanced Gain Characteristics of PbS-Doped Silica Fiber in O-Band by Co-Doping Er Ions

Xiuxiu Chen , Yanhua Dong , Jianxiang Wen , Hongyu Liu, Weizhu Ji , Xiangping Pan, Yanhua Luo , *Senior Member, IEEE*, and Tingyun Wang , *Member, IEEE*

Abstract—We report a novel PbS/Er co-doped silica fiber (PEDF) with improved spectral properties in O-band (1260–1360 nm). The results show that the gain of the PEDF exceeds 15 dB in the range of 1150–1360 nm. Compared to PbS-doped silica fiber, the PEDF has a gain improvement of 6.4–10.9 dB in O-band. In addition, the concentration of Pb and S in the PEDF core is significantly higher, and the size distribution of PbS nanoparticles is more concentrated in a narrow range. These factors may account for the enhanced gain characteristics of the PEDF. This work reveals the positive effect of co-doping Er^{3+} ions on the gain characteristics of the PEDF in O-band, and suggests an important research direction for the design of broadband amplifiers and light sources for optical communication with zero dispersion.

Index Terms—Broadband amplifiers, gain characteristics, PbS nanoparticles, PbS/Er co-doped silica fiber.

I. INTRODUCTION

EXPANDING the bandwidth of optical fiber amplifiers and enhancing the gain characteristics can improve the efficacy of communication systems [1], [2]. Erbium-doped fiber amplifiers and other rare-earth-doped fiber amplifiers can achieve high gain in specific wavelength bands. However, the gain bandwidths are usually limited because of the inherent energy-level structure of rare earth (RE) ions [3], [4]. Bi-doped fiber amplifiers exhibit broadband luminescence and amplification. However, the nature of Bi active centers remains controversial and it is difficult to control during the fabrication process. Hence, it is crucial to identify new materials for improving the optical properties of actively doped fibers in the near-infrared band.

Recently, nano-semiconductor materials with high quantum efficiency, bandgap tunability, and broad spectral properties have received widespread attention [5], [6]. Compared to other nano-semiconductors, those in the IV-VI group have significant advantages in the optical communication field because of the distinct energy level structure, smaller bulk band gap energy, and larger Bohr radius. In particular, PbS, with a bulk band gap energy and Bohr radius of 0.41 eV and 18 nm, respectively, has high fluorescence intensity and spectral stability, large Stokes shift, and strong quantum-limited effect [7]. The luminescence bands of the PbS-doped fibers include the low-loss communication window of 1.3 μm to 1.5 μm [8], [9]. However, PbS single-doped fibers cannot achieve a high gain. This is because PbS is temperature sensitive, easily diffuses and volatiles during the fiber fabrication, and result in a low effective doping concentration and low nucleation rate of PbS in the fiber cores. Moreover, controlling the size of PbS nano-semiconductors by thermal treatment method is challenging, as a slight increase in temperature will lead to the uncontrolled growth of nano-semiconductors.

The co-deposition of nano-semiconductors with other materials have been proposed to obtain desirable optical characteristics. In particular, co-doping with RE ions has received considerable research interest as a promising gain medium. Heo et al. investigated the effects of RE ions such as Ho^{3+}, Er^{3+}, and La^{3+} on the nucleation and optical characteristics of PbS nano-semiconductors in silicate glass during thermal treatment [10], [11]. They found that RE ions can serve as nucleation centers and reduce the size of PbS nano-semiconductors. By analyzing the energy dispersion spectra of Nd and PbS co-doped glass fiber, Park et al. discovered that Nd^{3+} can be located in the interior of PbS materials as Nd-O bonds [12]. These findings indicate that the introduction of RE ions contributes to the nucleation and growth of PbS. Wang et al. prepared PbS and Tm^{3+} co-doped glass fiber and achieved ultra-broadband luminescence at 1400–2600 nm [13]. Pan et al. discovered that co-doping Er^{3+} ions can enhance the local crystal field intensity and affect the local structure of the silica matrix based on theoretical studies [14]. However, the influences on the spectral characteristics near 1.3 μm was not considered in their work. Moreover, although numerous studies investigated the co-doping properties of RE ions and PbS nano-semiconductors, most of them only focused on size regulation and glass fibers. Few studies focused on the improvement of the fluorescence and gain characteristics of co-doped fibers, especially the doped silica fibers with advantages such as low loss and easy welding. Thus, a novel PbS/Er co-doped silica fiber (PEDF) is proposed by analyzing the co-doping effect of Er^{3+} ions on PbS-doped fibers.
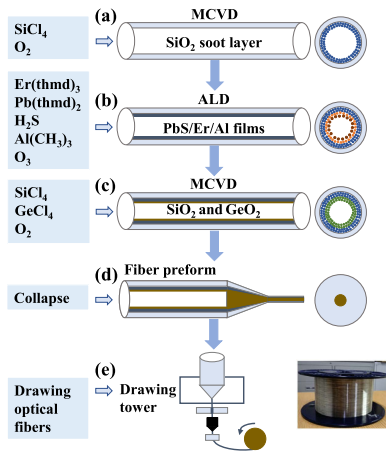
Fig. 1. Fabrication of the PbS/Er co-doped silica fiber. (a) deposition of soot layers on the inside surface of silica substrate tube. (b) deposition of PbS/Er/Al nanofilms on the surface of soot layers. (c) deposition of SiO_2 and GeO_2 materials in the silica substrate tube. (d) formation of the fiber preform, and (e) formation of the doped silica fiber.

In this study, PbS-doped silica fiber (PDF) and PEDF were fabricated via atomic layer deposition (ALD) combined with modified chemical vapor deposition (MCVD). The influences of co-doping Er^{3+} ions on the fiber properties of the PEDF was investigated in terms of the elemental composition, microstructure, and spectral properties.

II. EXPERIMENTAL SECTION

A. Optical Fiber Fabrication

ALD (Beneq TFS-200, Finland) and MCVD (Rosendahl Nextrom GmbH, Finland) [15] technologies were used to fabricate the PEDF, as shown in Fig. 1. First, $SiCl_4$ (42 sccm) and O_2 were blown into a cleaned silica substrate tube and oxidized via MCVD at approximately 1800 °C, to obtain SiO_2 soot layers on the inside surface of the silica substrate tube. The porous soot layers facilitate to optimize the homogeneity of the deposited materials [16]. A semi-glassing process was then performed at approximately 1400 °C. Second, Er_2O_3 (800 cycles), PbS (3000 cycles), and Al_2O_3 were alternately deposited onto the surface of the soot layers via ALD, and formed nanofilms. $Pb(tmhd)_2$ (tmhd: 22,66-tetramethyl-35-heptanedionato), H_2S gas (10% H_2S/N_2 mixture), $Er(tmhd)_3$, $Al(CH_3)_3$, and O_3 gas were used as reaction precursor materials for Pb, S, Er, Al, and O, respectively. The ALD process was reported in detail in literatures [14], [17], [18]. In addition, the deposited Al_2O_3 materials can serve as protective layers and reduce the volatilization of PbS to some extent, owing to the higher melting point and boiling point than PbS materials [19], [20]. Al_2O_3 can also improve the compatibility between PbS and silica substrates. Third, $SiCl_4$ (42 sccm), $GeCl_4$ (30 sccm) and O_2 were blown into the silica substrate tube via MCVD to obtain SiO_2 and GeO_2 materials. The deposited SiO_2 and GeO_2 can improve the refractive index of the fiber cores. After glassed at high temperature to form the inner fiber core and a collapse process occurred at approximately 2100–2200 °C. The fiber preform was formed. Then it was placed in the graphite furnace of the
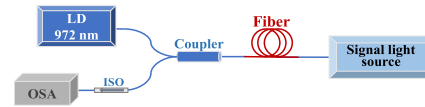
drawing tower and heated at 2000–2100 °C for approximately 0.5 h. Finally, the preform was drawn into PEDF. The drawing speed and tension were approximately 5–50 m/min and 1.5–2.5 N, respectively. The PDF without doped Er ions was fabricated under the same conditions.

Fig. 2. Experimental setup of the gain measurement of the fiber (LD: laser diode; ISO: isolator; OSA: optical spectrum analyzer).

B. Experimental Setup

Energy dispersive X-ray spectroscopy (EDS, MX80, Oxford Instruments, U.K.) was used to detect the content of each element in the fibers, and the electron energy used was 0–10 keV. An optical microscope (Olympus BX43, Japan) was used to observe the cross-sections of the fibers. The refractive index distribution and Raman spectra were measured using a fiber refractive index analyzer (S14, Photon Kinetics Inc., USA) and a confocal Raman microscope (LabRam HR800, Horiba Jobin Yvon, France), respectively. High-resolution transmission electron microscopy (HRTEM, JEM-2010F, Japan) with selected area electron diffraction (SAED) was used to examine the existential states and the distribution of the doped materials in the fiber cores.

Furthermore, the optical absorption spectra of the fibers were measured by the cut-back method. The fluorescence spectra were measured via backward pumping. The experimental setup of gain spectra is shown in Fig. 2. In this system, a 972 nm laser diode (LD) is used as the pump source, and the white light source (Yokogawa AQ4305, Japan) with broad-spectrum flat output serves as the signal source. In addition, the isolator (ISO) in the measurement system can prevent laser oscillation and protect the optical spectrum analyzer (OSA, Yokogawa AQ6370D, Japan). Its center wavelength is approximately 1310 nm. A coupler with the low loss characteristics near 1300 nm is used to couple pump light and signal light. In this work, the fibers used for fluorescence and gain measurements were approximately 10 m in length.

III. RESULTS AND DISCUSSION

A. Elemental Analysis

The atomic percentage (at%) of each element in the PDF and PEDF were determined and are listed in Table I. There are no Er^{3+} ions in the PDF, and the doping composition of Er^{3+} ions is approximately 0.015 at% in the PEDF. From the table, it can be discovered that the atomic percentages of both Pb and S in the PEDF are higher than that of PDF, which may be attributed to the influence of co-doping Er^{3+} ions. On one hand, the dense Er_2O_3 nanofilms prepared by ALD may be easily adsorbed on PbS materials during fiber fabrication, which can partially inhibit the volatilization of Pb and S at high-temperature [8], [21]. On the other hand, Er^{3+} ions may affect the re-nucleation process of PbS

TABLE I
ELEMENTAL CONTENT OF THE FIBER SAMPLES

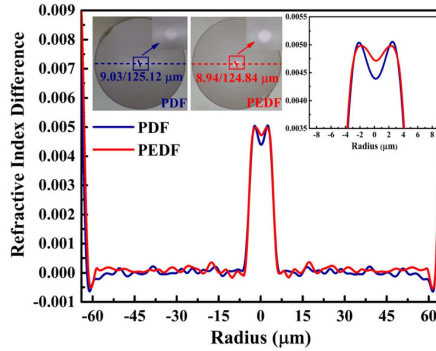| Element	PDF (at%)	PEDF (at%)
Er	/	0.015
Pb	0.014	0.021
S	0.016	0.024
Al	0.359	0.312
Ge	1.462	1.427
Si	32.835	33.733
O	65.314	64.468

Fig. 3. Refractive index distribution of the PDF and PEDF. The insets in the upper-left corner show the cross-sections of the fibers and the cores. The inset in the upper-right corner shows the enlarged refractive index distributions of the cores.

by forming Er-O bonds inside PbS, and the stability of the newly nucleated PbS may be enhanced [11], [12], [22]. Moreover, although the concentrations of the Ge, Si, and O deposited in the PDF and PEDF are slightly different, they are all within the acceptable range and do not affect the results of this study. In contrast, the percentage of Al in the PEDF is lower than that of PDF. Given that Al_2O_3 materials have the protective effect on PbS, it is determined that the increase of the PbS deposition concentration in the co-doped fibers may be mainly owing to the introduction of Er^{3+} ions.

B. Optical Characteristics

The cross-sections of the fibers were observed via optical microscopy, as shown in the insets of Fig. 3. The core and cladding diameters of the PDF and PEDF are 9.03/125.12 μm and 8.94/124.84 μm, respectively, consistent with the dimensions of single-mode fiber (SMF).

The refractive index distributions are shown in Fig. 3. The refractive index differences (RIDs) between the core and cladding of the PDF and PEDF are approximately 0.00431 and 0.00463, respectively. Using these data, the numerical aperture (NA)/cut-off wavelengths of the PDF and PEDF were calculated to be approximately 0.112/1.31 μm and 0.116/1.34 μm, respectively. The cut-off wavelengths of the fibers are relatively long and do not achieve the strict single-mode transmission in the whole O-band, which is the price for achieving low-loss fusion with SMF. However, the critical role of Er^{3+} ions can still be well highlighted due to the close cut-off wavelengths.

Depressions in the cores of the fibers were observed based on the refractive index profiles, which were caused by the
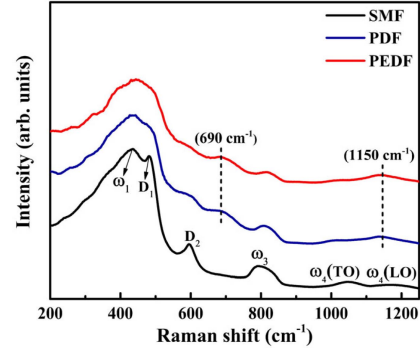

Fig. 4. Raman spectra of SMF, PDF, and PEDF.

volatilization of Ge at high-temperature. The higher refractive index of the PEDF core than that of PDF core, can be attributed to the introduction of Er^{3+} ions. The doped Er^{3+} not only directly increased the refractive index of the fiber core, but also indirectly improved the refractive index distribution of the co-doped fiber by improving the deposition efficiency of the PbS [23]. Furthermore, the addition of different dopants would not cause a significant change in the shape of the core, which can be seen from the insets of Fig. 3.

C. Raman Spectra

The Raman spectra of SMF (SMF-28, Corning Inc., USA), PDF, and PEDF in the range of 200–1250 cm^{-1} were measured using a 633 nm laser, as shown in Fig. 4. Several typical bands were observed for the SMF. The bands near 430 cm^{-1} (ω_1), 490 cm^{-1} (D_1), and 600 cm^{-1} (D_2) can be attributed to the deformation vibration of the Si-O-Si network, and the symmetric stretching modes of the quaternary and ternary rings of the SiO_4 tetrahedron, respectively [24], [25]. The band located at approximately 800 cm^{-1} (ω_3) can be attributed to the symmetric stretch vibration of bridging oxygen (BO) atoms in Si-O-Si bending vibrations [26]. The splitting of transverse optical phonons (TO) and longitudinal optical phonons (LO) resulted in the ω_4 bands at 1050 cm^{-1} and 1200 cm^{-1}.

Furthermore, the intensity of the bands at near 490 cm^{-1} and 600 cm^{-1} decreased in the PDF and PEDF. This indicates that the introduction of PbS materials disrupted the silica lattice structure, may resulting in more non-bridging oxygen (NBO) structures. The new bands appeared at near 690 cm^{-1} and 1150 cm^{-1}. The band at near 1150 cm^{-1} can be assigned to the stretching vibration in the SiO_4 tetrahedra with one oxygen next to Al^{3+} ions (Si–O–Al) [25]. The band at 690 cm^{-1} may be caused by Pb, PbO·Pb, 3PbO·Pb, or 4PbO·Pb, owing to the oxidation of anions in PbS materials [27], [28]. These results of Raman analysis further indicate that the PbS materials were doped into the silica structure of the PDF and PEDF. In the case of PbS doping, the structure of the silica lattice was modified and formed new bands. The newly formed band located at near 690 cm^{-1} was stronger in the PEDF, which may be related to the formation of Er-O bonds in the silica structure. They can serve as nucleation sites and facilitate the doping of PbS materials. Additionally, no
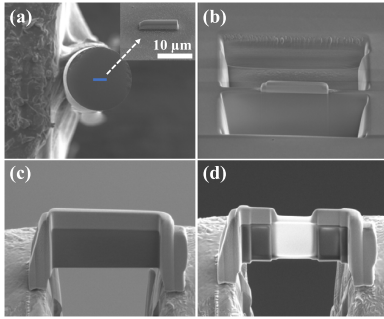
Fig. 5. Preparation process of HRTEM sample. (a) facet cutting and fiber fixing. (b) sampling with mechanical Pt probe. (c) fixed connection, and (d) trimming and thinning.
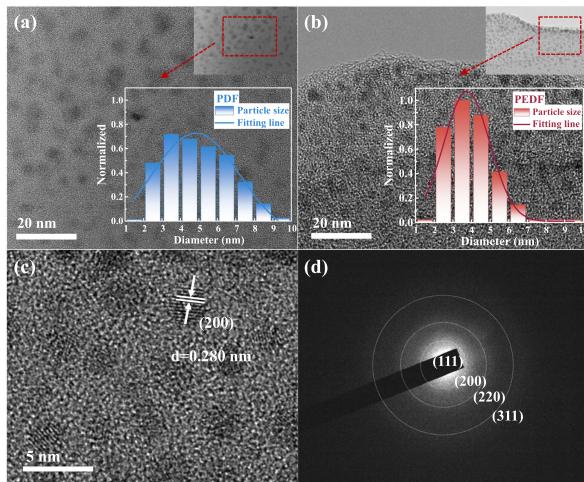

Fig. 6. HRTEM image and the particle size statistics of (a) the PDF sample and (b) PEDF sample. (c) Lattice image of the PEDF. (d) SAED patterns of the PEDF.

significant bands related to the PbS crystalline phase structure were detected, it is probably due to the low doping concentration of PbS and the fluorescence generated by the doped materials affect the characterization of PbS crystalline phase information.

D. HRTEM Images

The fibers were examined via HRTEM to analyze and confirm the distribution state and microstructure of the dopant materials in the cores. The samples for HRTEM analysis were prepared using Focused Ion Beam (FIB, 600i, FEI Hong Kong Co., Czekh) microdissection technology. The sample preparation processes mainly include cutting and fixing the fiber, spraying gold on the end face of the sample, collecting and fixing the sample, and trimming the sample, as shown in Fig. 5. Gold was sprayed to make the surface of the sample conductive. Pt protective films were usually sprayed on during processing to avoid damage the core area during ion-beam cutting. The size of the final sample for the HRTEM observation was approximately $10 \times 2 \times 3$ μm (length $\times$ width $\times$ height) and the thickness was less than 100 nm.

The results of HRTEM observations are shown in Fig. 6(a) and (b). Numerous nearly circular nanoparticles were existed

and uniformly distributed in the cores of the PDF and PEDF. According to previous studies [18], the deposited Er_2O_3 nanofilms exhibited amorphous or disordered structures. Therefore, the composition of the particles observed in the cores is tentatively considered to be PbS. Also, the PbS may be oxidized to form oxides such as PbO under the high temperature environment of the fiber fabrication process. The binding energy of PbS, approximately 161 eV, is larger than that of PbO, approximately 138 eV [29]. These indicate that PbS is more stable and easier to form than PbO. Therefore, the composition of the nanoparticles observed in the fiber core may be mainly PbS.

To determine the composition of the nanoparticles, the microstructure of the particles in the PEDF core was further investigated. The lattice stripe spacing of the particles in Fig. 6(c) is determined to be approximately 0.280 nm, which corresponds to the (200) crystal plane of PbS [30]. The diffraction rings observed via SAED are shown in Fig. 6(d), and correspond to the (111), (200), (220), and (311) planes of PbS [16], [30]. Thus, the analysis results confirm that the main component of the nanoparticles is PbS, which is present in the form of nanocrystal in the fiber core. This demonstrates that PbS nanoparticles were formed during the fiber fabrication process without subsequent heat treatment, reflecting the advantages of ALD combined with MCVD to fabricate PbS semiconductor-doped silica fiber.

In addition, particle size statistics were analyzed from 160–200 nanoparticles in the observation areas, and the corresponding statistical results are shown in the insets of Fig. 6(a) and (b). It was observed that the sizes of the PbS nanoparticles in the PDF and PEDF were small, in the range of approximately 2–10 nm. Further analysis of the particle size statistics revealed that the PbS nanoparticles in the PDF were distributed in the range of 2–8 nm, whereas the nanoparticles in the PEDF were more concentrated in the range of 2–5 nm. This may be attributed to the doping of Er^{3+} ions leading to PbS grain breakage, which causes a decrease in the crystallite size [31], [32]. Additionally, the difference in the size distribution of the PbS nanocrystals in optical fibers would result in the different spectral properties of the PDF and PEDF, owing to the quantum size effect of PbS nanocrystals [33], [34].

E. Absorption and Fluorescence Characteristics

The optical absorption characteristics of the PDF and PEDF were measured using the cut-back method, and the results are shown in Fig. 7(a). The background losses at 1300 nm were approximately 0.082 dB/m and 0.091 dB/m for the PDF and PEDF, respectively. The slightly higher background loss of the latter can be attributed to the presence of more nanoparticles in the PEDF core, which enhance Rayleigh scattering [35] and result in an increase in the transmission loss of the fibers. Additionally, six distinct absorption peaks were observed in the absorption spectrum of the PEDF at approximately 650, 800, 980, 1150, 1385, and 1535 nm. The absorption peak at 1385 nm is attributed to the OH overtone [36]. Combining the analysis of the absorption spectrum of the PDF and the typical absorption peaks of Er^{3+} ions, the peaks at 650 nm and 1535 nm correspond to the electron transitions of Er^{3+} ions, from the ground state $^4I_{15/2}$ to the excited states $^4F_{9/2}$ and $^4I_{13/2}$ [37],
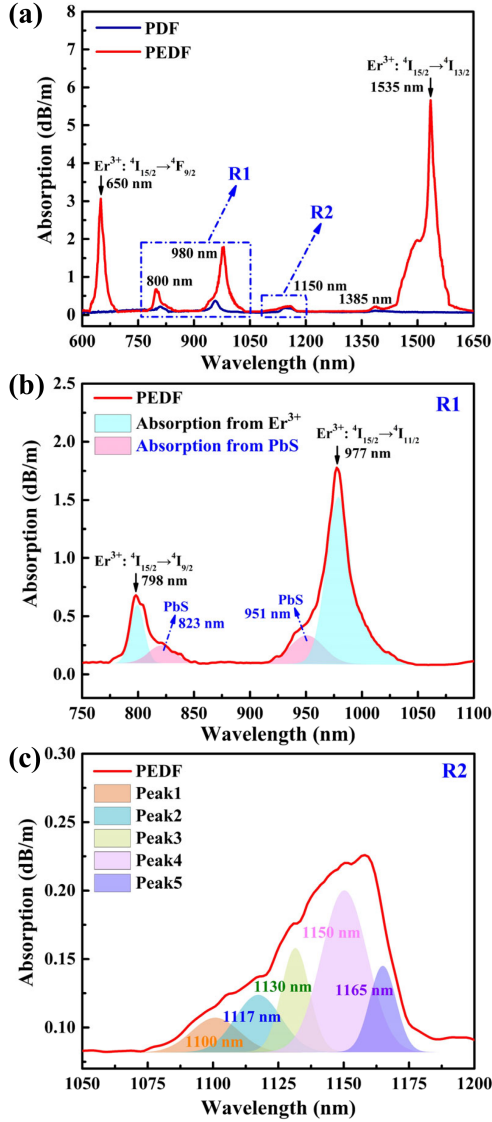
Fig. 7. (a) Absorption spectra of the PDF and PEDF. Gaussian fittings of the (b) R1 and (c) R2 regions for the PEDF absorption spectrum.
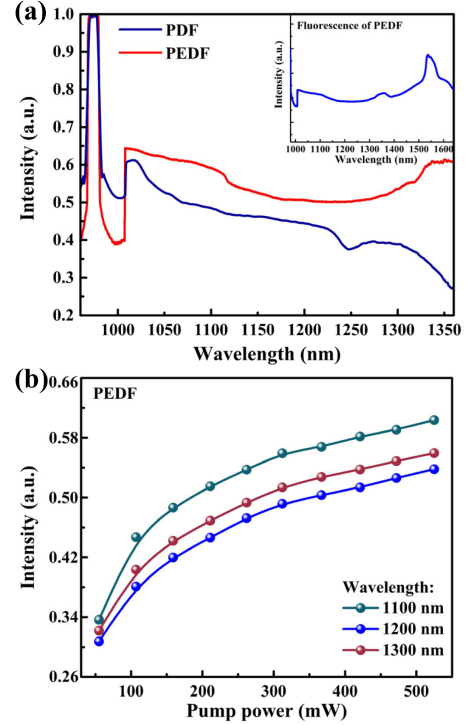

Fig. 8. (a) Fluorescence spectra of the PDF and PEDF. The inset shows the ultra-broadband fluorescence of the PEDF in the range of 1000–1600 nm. (b) Fluorescence intensity of the PEDF at different wavelengths versus the pump power.

respectively. The absorption bands at approximately 800 nm and 980 nm originate from the overlapping of the absorption peaks of PbS and Er^{3+} ions, and the band at approximately 1150 nm is attributed to the absorption by the PbS nanocrystals.

To further analyze and confirm the origins of the absorption bands at approximately 800, 980, and 1150 nm, two rectangular regions (R1 and R2) in Fig. 7(a) were magnified and processed using Gaussian fitting, as shown in Fig. 7(b) and (c), respectively. The results suggest that two absorption bands at near 800 nm and 980 nm originate from the superposition of the absorption peaks at approximately 798 (Er^{3+}: $^4I_{15/2} \rightarrow ^4I_{9/2}$) and 823 nm, and 951 and 977 nm (Er^{3+}: $^4I_{15/2} \rightarrow ^4I_{11/2}$), respectively. The absorption peaks at near 823 nm and 951 nm were caused by PbS materials, which are attributed to the formation of PbS nanocrystals with different sizes in the fiber core [38], [39], [40]. Based on the absorption intensity and effective mass method [41], the effective band gap energies and average radii of PbS nanoparticles at 823 nm and 951 nm can be estimated to be

approximately 1.51 eV and 3.07 nm, and 1.31 eV and 3.65 nm, respectively. In addition, based on the Gaussian fitting results and theoretical calculations, the absorption envelope near 1150 nm was determined to consist of several narrow absorption peaks at approximately 1100, 1117, 1130, 1150, and 1165 nm, with average radii of 3.82, 4.04, 4.43, 4.75, and 4.96 nm, respectively. These results are consistent with the size distribution (2–5 nm) of the PbS nanoparticles in the PEDF core from the HRTEM analysis.

Moreover, the absorption peaks caused by PbS nanoparticles were significantly enhanced in the PEDF. This is because the introduction of Er^{3+} ions generated nucleation sites for PbS, which promoting the effective formation of nanocrystals. Meanwhile, the effect of co-doping Er^{3+} ions on the size regulation of PbS nanocrystals resulted in a more concentrated size distribution. Thus, the absorption intensity of the PEDF at the wavelengths corresponding to these sizes was increased. This is beneficial for improving the performance of the PEDF.

According to the estimation of the particle sizes of the PbS nanoparticles, the corresponding luminescence centers were exactly in the broad spectral range of 1000–1400 nm [42]. This is consistent with the measured fluorescence spectra, as shown in Fig. 8(a). The PDF and PEDF exhibited broadband fluorescence from 1050 to 1360 nm, covering approximately 310 nm. This suggests that the broadband fluorescence of the PDF and PEDF near O-band is mainly owing to the presence of PbS nanoparticles with different sizes. The superposition of the luminescence centers at different wavelengths resulted in the broadband fluorescence phenomenon. In addition, the
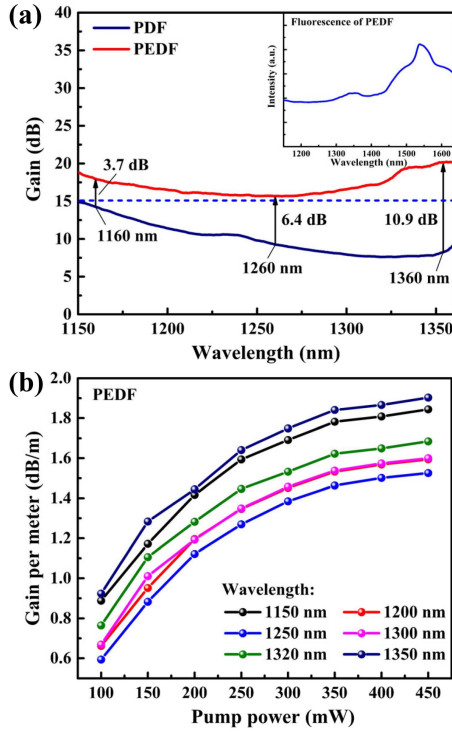
Fig. 9. (a) Gain spectra of the PDF and PEDF. The inset shows the ultra-broadband fluorescence of the PEDF in the range of 1150–1600 nm. (b) The gain per meter of the PEDF at different wavelengths versus pump power.

fluorescence of the PEDF was significantly enhanced compared to PDF, which indicates that co-doping Er^{3+} ions improved the spectral properties of the PEDF. Fig. 8(b) shows the variation in the fluorescence intensity at 1100, 1200, and 1300 nm with increasing pump power. The more intense fluorescence at 1100 nm and 1300 nm corresponds to a greater probability of PbS nanocrystals at the corresponding size distribution. Furthermore, owing to the superposition of the PbS and Er^{3+} ions lumines-cent bands, PEDF exhibited ultra-broadband fluorescence in the range of 1000–1600 nm, as shown in the inset of Fig. 8(a), which indicates that PEDF has excellent potential as a broadband light source.

F. Gain Characteristics

The broad-spectrum gain characteristics of the PEDF were further investigated based on its broad-spectrum fluorescence properties. To emphasize the effect of co-doping Er^{3+} ions on the gain performance of the PbS-doped fibers in O-band, the spectral characteristics in the range of 1150–1360 nm were examined.

Considering the effect of amplified spontaneous emission (ASE), the net gain (G_{net}) of the fiber can be calculated using the following equation [43]:

$$G_{net} = 10 \lg \left(\frac{P_{out} - P_{ASE}}{P_{in}} \right) \quad (1)$$

where P_{in}, P_{ASE}, and P_{out} denote the powers of the input optical signal, the ASE, and the amplified output optical signal,

respectively. The P_{ASE} is obtained by turning on the pump source while turning off the signal light source.

The broadband gain spectra of the PDF and PEDF are shown in Fig. 9(a) for the band of 1150–1360 nm. It is noteworthy that the gain of the PEDF exceeded 15 dB, which is an improvement of more than 3.7 dB compared to PDF. In particular, the gain in the whole O-band increased by 6.4–10.9 dB. These enhanced gain characteristics are very important for improving optical communication performance.

The gain spectra of the fiber at different wavelengths per unit length are shown in Fig. 9(b) to investigate the variation of the gain intensity of the PEDF according to the pump power. The intensity of the gain increased significantly when the pump power was low. This is attributed to the increased probability of carrier transition to higher energy levels in the core, which allows most carriers in the PbS nanocrystals to achieve inversion. The gain approached the saturation when the pump power was over 350 mW, at which point almost all the carriers were activated to high energy levels and additional inversion was not possible even if the pump power was increased. Co-doping with Er^{3+} ions is also shown to enhance the gain characteristics of PbS-doped fibers in O-band, which is achieved by increasing the effective doping efficiency and modulating the size of the PbS nanocrystals.

IV. CONCLUSION

In this work, the microstructure and spectral characteristics of the PEDF fabricated via ALD and MCVD are investigated. The positive effects of co-doping Er^{3+} ions on improving the performance of PbS-doped fibers are analyzed. The results show that the fluorescence and gain characteristics of the PEDF are significantly enhanced near 1.3 μm. In particular, the gain in-creases by 6.4–10.9 dB in the whole O-band. This phenomenon may be explained as follows. First, the deposited Er_2O_3 may be distributed around PbS nanocrystals, which can act as protective films to reduce the volatilization of PbS materials at high temper-ature and improve the effective doping concentration of Pb and S. Second, the co-doping Er^{3+} ions can form Er-O bonds and serve as nucleation sites, which may be favorable to the nucleation and size reduction of PbS nanocrystals, and resulting in a more concentrated distribution in the PEDF core. These can improve the luminescence efficiency and gain intensity near O-band. Therefore, the semiconductor and RE ions co-doped silica fiber used in this study has excellent potential in long-range, high-capacity communication networks and optical devices, such as broadband amplifiers and broadband light sources.

REFERENCES

[1] A. Donodin, V. Dvoyrin, E. Manuylovich, L. Krzczanowicz, and S. Turitsyn, "Bismuth doped fibre amplifier operating in E- and S- op-tical bands," *Opt. Mater. Exp.*, vol. 11, no. 1, pp. 127–135, 2021, doi: 10.1364/ome.411466.

[2] G. Xiao, B. Yan, Y. Luo, J. Wen, and G. D. Peng, "Co-doping ef-fect of lead or erbium upon the spectroscopic properties of bismuth doped optical fibres," *J. Lumin.*, vol. 230, no. 1, 2021, Art. no. 117726, doi: 10.1016/j.jlumin.2020.117726.

[3] G. Li, L. Li, X. Huang, J. Tang, and Q. Jiao, "Er^{3+} doped and Er^{3+}/Pr^{3+} co-doped gallium-antimony-sulphur chalcogenide glasses for infrared applications," *Opt. Mater. Exp.*, vol. 6, no. 12, pp. 3849–3856, 2016, doi: 10.1364/ome.6.003849.

[4] Z. Zheng, X. Pan, W. Ji, Y. Dong, J. Wen, and T. Wang, "Co-doping effect of Bismuth ions on the gain characteristics of Er-doped silica optical fiber," *IEEE Photon. J.*, vol. 14, no. 4, Aug. 2022, Art. no. 7146308, doi: 10.1109/jphot.2022.3193901.

[5] W. W. Yu, J. C. Falkner, B. S. Shih, and V. L. Colvin, "Preparation and characterization of monodisperse PbSe semiconductor nanocrystals in a noncoordinating solvent," *Chem. Mater.*, vol. 16, no. 17, pp. 3318–3322, 2004, doi: 10.1021/cm049476y.

[6] J. M. Pietryga, D. J. Werder, D. J. Williams, J. L. Casson, R. D. Schaller, and V. I. Klimov, "Utilizing the lability of lead selenide to produce heterostructured nanocrystals with bright, stable infrared emission," *J. Amer. Chem. Soc.*, vol. 130, no. 14, pp. 4879–4885, 2008, doi: 10.1021/ja710437r.

[7] N. Zhao and L. Qi, "Low-temperature synthesis of star-shaped PbS nanocrystals in aqueous solutions of mixed cationic/anionic surfactants," *Adv. Mater.*, vol. 18, no. 3, pp. 359–362, 2006, doi: 10.1002/adma.200501756.

[8] X. Huang, Z. Fang, and Z. Peng, "Formation, element-migration and broadband luminescence in quantum dot-doped glass fibers," *Opt. Exp.*, vol. 25, no. 17, pp. 19691–19700, 2017, doi: 10.1364/oe.25.019691.

[9] X. Tong, Y. Zhou, and L. Jin, "Heavy metal-free, near-infrared colloidal quantum dots for efficient photoelectrochemical hydrogen generation," *Nano Energy*, vol. 31, pp. 441–449, 2017, doi: 10.1016/j.nanoen.2016.11.053.

[10] X. Kai and J. Heo, "Lead sulfide quantum dots in glasses controlled by silver diffusion," *J. Non-Cryst. Solids*, vol. 358, no. 5, pp. 921–924, 2012, doi: 10.1016/j.jnoncrysol.2012.01.007.

[11] M. A. Kim, Y. K. Kwon, C. Liu, and J. Heo, "Lead sulfide quantum dots in glasses containing rare-earth ions," *J. Non-Cryst. Solids*, vol. 383, pp. 173–175, 2014, doi: 10.1016/j.jnoncrysol.2013.04.030.

[12] W. J. Park, M. G. Kim, J. E. Kim, J. Wang, H. J. Lee, and C. G. Park, "Role of Nd^{3+} ions on the nucleation and growth of PbS quantum dots (QDs) in silicate glasses," *J. Amer. Ceram. Soc.*, vol. 100, no. 7, pp. 2879–2884, 2017, doi: 10.1111/jace.14825.

[13] W. Wang, Y. Xiao, B. Zhou, S. Xu, and Q. Zhang, "Quantum-dots-precipitated rare-earth-doped glass for ultra-broadband mid-infrared emissions," *J. Amer. Ceram. Soc.*, vol. 102, no. 4, pp. 1560–1565, 2018, doi: 10.1111/jace.16259.

[14] X. Pan et al., "Improved fluorescence and gain characteristics of Er-doped optical fiber with PbS nanomaterials co-doping," *Materials*, vol. 15, no. 17, 2022, Art. no. 6090, doi: 10.3390/ma15176090.

[15] J. Wen et al., "Photoluminescence properties of Bi/Al-codoped silica optical fiber based on atomic layer deposition method," *Appl. Surf. Sci.*, vol. 349, pp. 287–291, 2015, doi: 10.1016/j.apsusc.2015.04.138.

[16] Y. Shang, J. Wen, Y. Dong, H. Zhan, Y. Luo, and G.-D. Peng, "Luminescence properties of PbS quantum-dot-doped silica optical fibre produced via atomic layer deposition," *J. Lumin.*, vol. 187, pp. 201–204, 2017, doi: 10.1016/j.jlumin.2017.03.009.

[17] X. Pan, Y. Dong, M. Jia, J. Wen, C. Su, and T. Wang, "Temperature-induced PbS quantum dots with tunable broadband wavelength grown by atomic layer deposition," *Appl. Surf. Sci.*, vol. 546, 2021, Art. no. 149086, doi: 10.1016/j.apsusc.2021.149086.

[18] T. Wang, X. Chen, X. Pan, Y. Dong, J. Wen, and M. Jia, "Efficient structural manipulation of PbS in Er-doped silica optical fibers for enhanced amplification systems," *J. Lumin.*, vol. 257, 2023, Art. no. 119689, doi: 10.1016/j.jlumin.2023.119689.

[19] T. Haruna, J. Iihara, K. Yamaguchi, Y. Saito, and T. Murata, "Local structure analyses around Er^{3+} in Er-doped fiber with Al co-doping," *Opt. Exp.*, vol. 14, no. 23, pp. 11036–11042, 2006, doi: 10.1364/oe.14.011036.

[20] F. Z. Tang, P. Mcnamara, G. W. Barton, and S. P. Ringer, "Nanoscale characterization of silica soots and aluminium solution doping in optical fibre fabrication," *J. Non-Cryst. Solids*, vol. 352, no. 36–37, pp. 3799–3807, 2006, doi: 10.1016/j.jnoncrysol.2006.06.014.

[21] X. Huang et al., "Controllable fabrication of novel all solid-state PbS quantum dot-doped glass fibers with tunable broadband near-infrared emission," *J. Mater. Chem. C*, vol. 5, no. 31, pp. 7927–7934, 2017, doi: 10.1039/c7tc02623d.

[22] S. M. Shim, C. Liu, Y. K. Kwon, and J. Heo, "Lead sulfide quantum dots formation in glasses controlled by erbium ions," *J. Amer. Ceram. Soc.*, vol. 93, no. 10, pp. 3092–3094, 2010, doi: 10.1111/j.1551-2916.2010.04045.x.

[23] X. Pan et al., "Enhanced FBG temperature sensitivity in PbS-doped silica optical fiber," *J. Lightw. Technol.*, vol. 37, no. 18, pp. 4902–4907, Sep. 2019, doi: 10.1109/jlt.2019.2937138.

[24] M. S. Wong, D. Hwang, A. I. Alhassan, C. Lee, R. Ley, and S. Nakamura, "High efficiency of III-nitride micro-light-emitting diodes by sidewall passivation using atomic layer deposition," *Opt. Exp.*, vol. 26, no. 16, pp. 21324–21331, 2018, doi: 10.1364/oe.26.021324.

[25] Y. Jiao, M. Guo, R. Wang, C. Shao, and L. Hu, "Influence of Al/Er ratio on the optical properties and structures of Er^{3+}/Al^{3+} co-doped silica glasses," *J. Appl. Phys.*, vol. 129, no. 5, 2021, Art. no. 053104, doi: 10.1063/5.0025398.

[26] G. S. Henderson, D. R. Neuville, B. Cochain, and L. Cormier, "The structure of GeO_2-SiO_2 glasses and melts: A Raman spectroscopy study," *J. Non-Cryst. Solids*, vol. 355, no. 8, pp. 468–474, 2009, doi: 10.1016/j.jnoncrysol.2009.01.024.

[27] J. L. Blackburn, H. Chappell, J. M. Luther, A. J. Nozik, and J. C. Johnson, "Correlation between pphotooxidation and the appearance of Raman scattering bands in lead chalcogenide quantum dots," *J. Phys. Chem. Lett.*, vol. 2, no. 6, pp. 599–603, 2011, doi: 10.1021/jz2000326.

[28] T. Tohidi, K. Jamshidi-Ghaleh, A. Namdar, and R. Abdi-Ghaleh, "Comparative studies on the structural, morphological, optical, and electrical properties of nanocrystalline PbS thin films grown by chemical bath deposition using two different bath compositions," *Mater. Sci. Semicond. Process.*, vol. 25, pp. 197–206, 2014, doi: 10.1016/j.mssp.2013.11.028.

[29] N. R. Mathews, C. ángeles–Chávez, M. Cortés-Jácome, and J. T. Antonio, "Physical properties of pulse electrodeposited lead sulfide thin films," *Electrochimica Acta*, vol. 99, pp. 76–84, 2013, doi: 10.1016/j.electacta.2013.03.044.

[30] F. Yue, J. W. Tomm, D. Kruschke, P. Glas, K. A. Bzheumikhov, and Z. C. Margushev, "PbS: Glass as broad-bandwidth near-infrared light source material," *Opt. Exp.*, vol. 21, no. 2, pp. 2287–2296, 2013, doi: 10.1364/oe.21.002287.

[31] K. Bouras, J.-L. Rehspringer, G. Schmerber, H. Rinnert, and S. Colis, "Optical and structural properties of Nd doped SnO_2 powder fabricated by the sol-gel method," *J. Mater. Chem. C*, no. 2, no. 2, pp. 8235–8243, 2014, doi: 10.1039/C4TC01202J.

[32] M. C. Portillo, O. P. Moreno, R. Pérez, R. P. Merino, H. S. Juarez, and S. T. Cuapa, "Characterization and growth of doped-PbS in situ with Bi^{3+}, Cd^{2+} and Er^{3+} ions by chemical bath," *Mater. Sci. Semicond. Process.*, vol. 71, pp. 22–31, 2017, doi: 10.1016/j.mssp.2017.09.012.

[33] J. Xue, X. Wang, J. H. Jeong, and X. Yan, "Fabrication, photoluminescence and applications of quantum dots embedded glass ceramics," *Chem. Eng. J.*, vol. 383, 2019, Art. no. 123082, doi: 10.1016/j.cej.2019.123082.

[34] F. Arquer, D. V. Talapin, V. I. Klimov, Y. Arakawa, and E. H. Sargent, "Semiconductor quantum dots: Technological progress and future challenges," *Science*, vol. 373, no. 6555, 2021, Art. no. eaaz8541, doi: 10.1126/science.aaz8541.

[35] V. Fuertes, N. Grégoire, P. Labranche, S. Gagnon, and Y. Messaddeq, "Engineering nanoparticle features to tune Rayleigh scattering in nanoparticles-doped optical fibers," *Sci. Rep.*, vol. 11, no. 1, pp. 1–12, 2021, doi: 10.1038/s41598-021-88572-2.

[36] I. Moreels, D. Kruschke, P. Glas, and J. W. Tomm, "The dielectric function of PbS quantum dots in a glass matrix," *Opt. Mater. Exp.*, vol. 2, no. 5, pp. 496–500, 2012, doi: 10.1364/ome.2.000496.

[37] Y. Luo, J. Wen, J. Zhang, J. Canning, and G.-D. Peng, "Bismuth and erbium codoped optical fiber with ultrabroadband luminescence across O-, E-, S-, C-, and L-bands," *Opt. Lett.*, vol. 37, no. 16, pp. 3447–3449, 2012, doi: 10.1364/ol.37.003447.

[38] H. Wang, G. Wu, and J. Qiu, "Direct evidence on the energy transfer of near-infrared emission in PbS quantum dot-doped glass," *Opt. Exp.*, vol. 23, no. 13, pp. 16723–16729, 2015, doi: 10.1364/oe.23.016723.

[39] Y. Xiong, C. Liu, and J. Wang, "Near-infrared anti-stokes photoluminescence of PbS qds embedded in glasses," *Opt. Exp.*, vol. 25, no. 6, pp. 6874–6882, 2017, doi: 10.1364/oe.25.006874.

[40] J. Zheng, Y. Dong, X. Pan, J. Wen, and Z. Chen, "Ultra-wideband and flat-gain optical properties of the PbS quantum dots-doped silica fiber," *Opt. Exp.*, vol. 27, no. 26, pp. 37900–37909, 2019, doi: 10.1364/oe.27.037900.

[41] Y. Wang, A. Suna, W. Mahler, and R. Kasowski, "PbS in polymers. From molecules to bulk solids," *J. Chem. Phys.*, vol. 87, no. 12, pp. 7315–7322, 1987, doi: 10.1063/1.453325.

[42] Y. Dong et al., "Numerical analysis of noise and gain equalisation characteristics of few-mode PbS quantum dots-doped silica fibre amplifier," *Opt. Commun.*, vol. 517, 2022, Art. no. 128240, doi: 10.1016/j.optcom.2022.128240.

[43] J. Vallés, A. Ferrer, J. M. Fernández-Navarro, V. Berdejo, and J. Solís, "Performance of ultrafast laser written active waveguides by rigorous modeling of optical gain measurements," *Opt. Mater. Exp.*, vol. 1, no. 4, pp. 564–575, 2011, doi: 10.1364/ome.1.000564.